IAC-24-C2.4.2.x88721

On the Impact of Gravity During the Micro-Vibration Characterization of Reaction-Wheels: An Experimental Assessment

Matias Bestard Körner^{a*}

^a German Aerospace Center (DLR), Institute of Space System, Navigation and Control Systems, Robert-Hooke-Strasse 7, 28359 Bremen, Germany, matias.koerner@dlr.de

Abstract

Spacecraft operating in orbit rely on a disturbance-free environment to achieve the designated mission goals spanning between remote systems for observation and communication purposes or special micro-gravity missions. They require pointing mechanisms to target, for example, a star or a patch of land on Earth or to maintain operation without unnecessarily changing the attitude, a representative example being reorienting solar panels according to an orbit. An accurate pointing generally requires components like motors or rotating masses for attitude control systems: they generate disturbances, also called micro-vibrations, alongside the whole vehicle, often resulting in jitter if not mitigated. As such, it is crucial to characterize the disturbance source to study the mitigation possibilities and reduce their impact in later operations.

A common practice to characterize reaction-wheels is to mount them on dynamometers to measure the forces and torques generated over a wide bandwidth, with the rotation axis aligned with the gravity vector. In contrast, another possibility is to perform tests using reaction-wheels on an integrated or semi-integrated spacecraft in a flight-comparable configuration. However, combining and applying both methods during spacecraft or mechanism development may leave some dynamics unmodeled and uncertainties omitted. These uncertainties result from the many different system mechanical configurations available in the spacecraft development cycle and the impact of gravity on the structures and actuators under test.

In this study, we focus on the impact of changing the gravity-vector direction during the characterization of reaction-wheels in a laboratory by comparing the results under varying conditions. Specifically, the method measures the generated micro-vibrations against the gravity vector with a rotating measurement setup, including a dynamometer and the reaction-wheel under test. The feasibility of this method for characterizing small- and medium-sized reaction-wheels is explored, including a range of possible configurations. Additionally, we discuss tools and methods used to compare test cases and recorded vibration data. Consequently, this method allows the validation and verification of further simulations, numerical models, or tests during a spacecraft's design lifecycle up to assembly and integration. In a broader context, this investigation shows the test possibilities to be considered while developing new space systems and actuators, especially as the latter get more complex in geometry or design of the components assembly.

Keywords: micro-vibration, jitter, reaction-wheel, test, characterization, gravity

Acronyms/Abbreviations

DAQ Data Acquisition System
DUT Device Under Test

FFT Fast Fourier Transformation

IQR Interquartile Range

PE Pulse Event
Q1 First Quartile
Q4 Fourth Quartile
RMS Root Mean Square
RPM Round Per Minute

RTOS Real Time Operating System

1. Introduction

The accurate pointing of spacecraft in orbit is crucial for achieving mission goals, whether observing remote systems, maintaining communication, or conducting scientific experiments. Spacecraft rely on disturbance-free environments and precise attitude control systems to ensure their instruments are accurately pointed at the desired target. However, these systems may generate micro-vibrations, mainly when reaction-wheels are used, resulting in line-of-sight jitter if not mitigated [1]. Micro-vibrations are generally of a limited amplitude level, hence, not endangering the structural integrity, but still may result in loss of mission performance [2]. Therefore, it is essential to characterize these vibrations and mitigate their impact.

To ensure accurate pointing, space system developers and equipment suppliers have employed several methods for characterizing reaction-wheels, including dynamometer-based measurements. Alternatively, other approaches involve performing tests using integrated or semi-integrated spacecraft in flight-

IAC-24-C2.4.2.x88721 Page 1 of 12

^{*} Corresponding Author

comparable configurations. However, combining these methods may still result in some unmodeled dynamics and uncertainties, like the difficulty of deploying or integrating solar arrays, appendages, or elements that may amplify micro-vibrations due to physical limitations or components still in development [1][2]. However, the dynamometer-based measurements may not be sufficient to capture all possible effects occurring during spacecraft operations, especially micro-gravity.

In this study, we aim to investigate the impact of changing the gravity-vector direction during the characterization of reaction-wheels in a laboratory setting by comparing results under varying conditions. Specifically, our method involves measuring generated micro-vibrations against the gravity vector using a rotating measurement setup, including a dynamometer and the reaction-wheel under test, as shown in Figure 1. In detail, this method has been investigated in a previous study [3], in which the setup was thoroughly tested for its validity to measure micro-vibrations under a rotating gravity vector, using a reference test actuator to stimulate the entire measurement range of the setup.

We explore the feasibility of this method for characterizing small- to medium-sized reaction-wheels, considering various configurations. We also discuss tools and methods for comparing test cases and recorded vibration data. This approach enables the validation and verification of further simulations, numerical models, or tests during a spacecraft's design lifecycle up to assembly and integration.

In a broader context, our investigation highlights the importance of considering test possibilities when developing new space systems and actuators, especially as they become more complex in geometry or component assembly design.

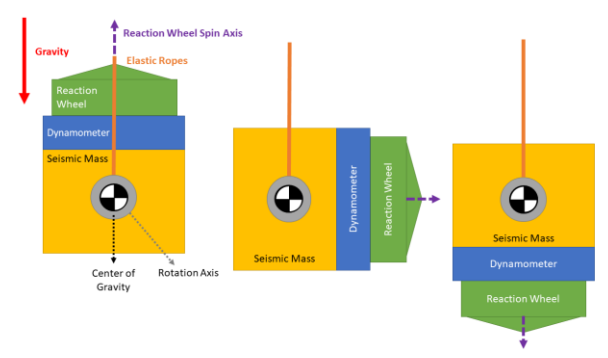


Figure 1: Experimental concept with the rotation of the reaction-wheel spin axis against the gravity vector

1.1 Dynamometer Based Measurements

Dynamometers are precision instruments that measure the forces and torques generated by a moving component, such as a reaction-wheel with its motors, bearings, and flywheel. In these tests, the reaction-wheel is mounted on a dynamometer, and its flywheel spin

axis is aligned with the gravity vector and, hence, levelled. The resulting measurements provide valuable insights into the wheel's performance, including torque output, speed response, and vibration characteristics. [2]

However, dynamometer tests have limitations when used to characterize reaction-wheels individually or once assembled into semi-integrated spacecraft configurations. First, dynamometers are typically designed for individual component testing, making capturing the behaviour of a more significant number of reaction-wheels over extended periods costly. It also makes testing challenging for reactionwheel assemblies that are only operational once tightly integrated with other components or structures. Moreover, the actual operating environment of a spacecraft can be challenging to replicate on a dynamometer, such as the dynamic mass response [2], leading to uncertainties in the measurements and potentially causing issues that may arise during integrated system tests or as late as actual flight operation. Also, the dynamometers typically focus on individual component behaviour, neglecting potential interactions with other parts of the system that could affect the overall performance, for example, such as the interaction between several reaction-wheels.

These limitations highlight the need for alternative methods or approaches to characterizing reaction-wheels analogous to those in semi-integrated spacecraft configurations or under flight operations conditions.

As mentioned, the dynamometer is levelled and aligned with the gravity vector, meaning there is uncertainty regarding the performance once the wheel operates in micro-gravity, especially if non-linear effects and bearing dynamics are considered. Additionally, dynamometers are typically designed to operate in a controlled environment with known forces and moments, which may not accurately reflect a spacecraft's overall environmentally dynamic behaviour during operation. Future Space missions may include inflight measurements and tests that, in consequence, may prove beneficial to validating the testing using dynamometers. [1][4][5].

2. Material and methods

2.1 Measurement Principle

The measurement principle employed in this study is based on the one described in a previous study [3]. This approach involves rotating the gravity vector around the setup to create a controlled environment that changes the reaction-wheel's gravity. In contrast to the microgravity approach, this method provides the change of a single test variable without requiring an entire microgravity test facility, such as a parabolic flight or droptower facility, with a higher repeatability expectation

IAC-24-C2.4.2.x88721 Page 2 of 12

due to the Test happening in a highly controlled laboratory environment.

The previous study demonstrated that this measurement technique is effective for characterizing the behaviour of inertial actuators under different gravitational conditions. The method involves measuring the forces and torques at the mechanical interface of the unit to be characterized, which in our case is a reaction-wheel, using a dynamometer attached to a large seismic mass suspended in isolation in the laboratory. The reaction-wheel is operated at specified speeds to evaluate the forcing functions generated and, consequently, the micro-vibration profile.

2.2 Experimental Setup

Several components were employed to achieve the experimental setup with the gravity rotation requirement. A Kistler 9236A1 piezoelectrical multicomponent dynamometer was used to measure the forces acting from the Device Under Test (DUT), a reaction-wheel. At the same time, a Kistler 5080A 8-channel charge amplifier amplified the output signal from the dynamometer and sent it to the data acquisition system. The Kistler 5697A data acquisition system recorded the amplified signals, providing 12 measurement channels from the dynamometer load cells. A stainless-steel block served as a seismic mass to support the dynamometer measurement.



Figure 2: Suspended setup (Setup-A) in an upright position, with a dynamometer mounted on top of the seismic mass (grey) fixed with slings to elastic ropes. The reaction-wheel (black) is mounted on the top of the dynamometers ceramic plate (white).

As shown in Figure 2, the setup is suspended from the laboratory ceiling using elastic ropes adaptable in length to tune the lower harmonic frequencies and provide a certain degree of isolation and dampening. Slings serve as an interface between the elastic ropes and the rotation axis on the seismic mass, keeping the block's rotation angle by friction and allowing fine

adjustments with the use of a precision digital spirit level between tests.

The measurement equipment is configured in three different setups with varying conditions, each with a level tolerance of 0.5 degrees against the intended direction:

- <u>Setup-A:</u> The measurement equipment is upright, and the DUT is on top.
- <u>Setup-B:</u> The measurement equipment is tilted 90 degrees with the DUT hanging on the side.
- <u>Setup-C:</u> The measurement equipment faces downwards with the DUT hanging below it.

The measurement data consists of the forces and torques exerted by the DUT against the dynamometer interface and, consequently, against the seismic mass. By analysing the data collected from these setups, we can gain insights into how the gravity vector affects the behaviour of the actuator unit.

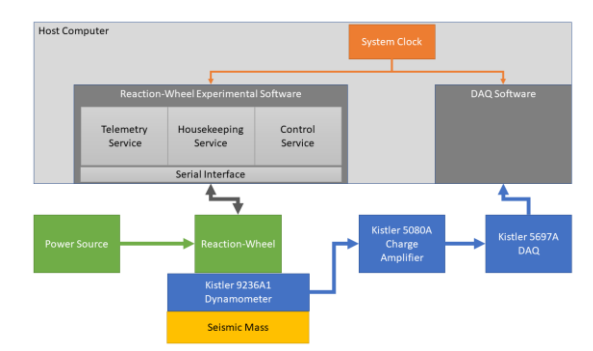


Figure 3: Signal chain of the setup: control signals in green, measurements in blue, telemetry/telecommand in grey, clock signal in orange

The experimental setup is controlled from a host computer, as represented in Figure 3. One of the main difficulties for the time-data processing emerging from the setup is time-synchronization, especially if event timing and correlation are required. The dynamometer measurement chain has an internal buffer and outputs the measurements to the DAQ software, which uses timestamps from the host computer's system clock. On the other hand, the reaction-wheel is controlled using custom software running on a different processing thread on the Host Computer. The Host Computer is not running a Real-Time Operation System (RTOS). Hence, synchronicity between the software modules is not guaranteed, possibly leading to additional postprocessing effort regarding the recorded data generated by the timestamps Reaction-Wheel Experimental Software and the DAQ Software.

2.3 Reaction-Wheel Unit under Test

The Device Under Test in this study was a mediumsized model reaction-wheel. The specific wheel type is optimized to operate under laboratory conditions, but it

IAC-24-C2.4.2.x88721 Page 3 of 12

is compatible with space-operated designs. A total of 4 reaction-wheels are available for this setup such that, in future, further tests can be performed to rule out single individual effects, e.g. caused by defects or damage, can be ruled out. Due to proprietary reasons, the exact model of the device and its precise characteristics are not disclosed. However, approximate values represent its typical operational capabilities, as seen in Table 1.

Table 1. Device Under Test approximate properties with a tolerance of 20%.

| Reaction-Wheel | | | | |
|----------------------------|-------------------------|--|--|--|
| DUT-Mass | 3 kg | | | |
| Rotating Moment of Inertia | 0.007 kg·m ² | | | |
| Operational Torque | 0.900 N⋅m | | | |
| Operational Speed Domain | +/- 6000 rpm | | | |
| Max. Power Consumption | 160 W | | | |

The wheel's central axis of rotation, as seen in Figures 1 and 2, was set perpendicular to the dynamometer's ceramic interface plate. An adapter has been designed and optimized to interface between the reaction-wheel interface hole pattern and the dynamometer hole pattern.

The reaction-wheel's control software, Reaction-Wheel Experimental Software, runs on the Host Computer. This software constantly generates telemetry and housekeeping requests for the reaction-wheel motor control unit. Over a User Interface, the experiment director can command individual states, like targeted RPM goals or torques, over a User Interface or trigger a pre-defined test command sequence. A serial interface provides communication for the telemetry data, housekeeping data and telecommand requests. The reaction-wheel motor control unit inside the assembly processes the requests and commands and drives the reaction-wheel motor. In the background, the Reaction-Wheel Experimental Software logs and recodes the communication and decoding of the telemetry and housekeeping data.



Figure 4: Suspended Setup-B (Left) and Setup-C (Right) as set up during the test execution.

2.4 Test Execution

The test steps executed in this study were designed to excite the wheel in different operational conditions. The test steps were designed to simulate various scenarios that would be encountered during actual space missions. These included:

- Preparing the corresponding Test-Setup (A, B, or C, as seen in Figures 2 and 4.)
- Generating a torque Pulse-Event (PE)
- Performing a continuous rotation measurement
- Change to the next corresponding Test-Setup

2.4.1 Generating a Pulse-Event (PE)

The pulse event generates a torque on the wheel that briefly rotates it in one direction. The goal of this part of the Test is twofold. First, the pulse can be used to evaluate the system response of both the reaction-wheel controller and the structural response. Second, similar events may happen if a slight imperfection in the reaction-wheel bearing system causes a sudden drop in the wheel speed (RPM) and the reaction-wheel controller catches up with a torque command spike.

The control software generates a command to torque the wheel in one direction for a brief period, namely a single telecommand cycle of the wheel's internal controller (not to be confused with the internal control loop period of frequency) to accomplish the Pulse Event. After the initial command, the control software would prompt a "MOTOR OFF" command to stop the controller and make the wheel rotate freely (idle). While the event pulse length is commanded with a 10 milliseconds resting period, the response of the motor controller is known to be slower.

During the Pulse-Event phase, the Dynamometer and DAQ systems record the forces and torques generated. The pulse event's result is later analysed in the results section.

2.4.2 Continuous rotation measurement

The continuous rotation measurement portion of this Test examines the reaction-wheel's nominal operation, which is similar to its function on a spacecraft. The wheel was commanded to rotate at a constant speed, starting from 0 RPM and increasing in increments of 200 RPM up to a maximum speed of 6000 RPM.

The internal motor control loop was utilized to achieve the target speed. The target rotational speed (RPM) was commanded by the Host Computer—Reaction-Wheel Experimental Software, then acknowledged and set by the controller, and the motor accelerated the wheel until it reached that speed. Once the desired speed was attained, the motor controller maintained the wheel's rotation at that constant rate. The same sequence of commands was used for all three test cases (with setups A, B, and C).

3. Data Processing

Due to proprietary constraints, the raw and fully processed data are not disclosed in this study. However, selected results have been normalised or adjusted to

IAC-24-C2.4.2.x88721 Page 4 of 12

provide a qualitative assessment within the scope of this research.

As indicated in Section 2, the recorded data from both the dynamometer and the reaction-wheel are present in the time domain. The first step is to establish and validate the synchronicity of the datasets. Afterwards, the datasets are chunked into individual timeframes corresponding to either the individual test steps, the Pulse Event execution, or the individual continuous rotation measurements.

The individual continuous rotation measurements are selected when the rotation speed has been reached, and the residual translation and rotation motions caused by the torque generated to reach a certain RPM have ceased. The exact timeframe is established empirically since no automatized system is implemented in the setup. The conditions are established by observation that the target RPM has been reached for at least 10 seconds and that the RPM increases are happening at a lower rate than 200 RPM per 10 seconds.

3.1 Pulse Event Data

Due to the pulse event's transient nature, the initial assessment and analysis are done in the time domain. Once the validity of the time domain data is established, both during the live preview of the dynamometer output at the test time and later after the more in-depth data correlation with the motor controller telemetry, the frequency domain analysis is performed with an FFT.

3.2 Continuous Rotation Measurement Data Processing

The analysis of the recorded data will be limited to frequency domain analysis in this study since one of the goals is to provide qualitative insight into the different test cases. Moreover, the observation of transient effects would require more extended measurement periods and exceed the scope of the study.

The data from the continuous rotation measurements is processed for the three individual cases. First, the force and torque vector magnitudes are computed from the individual dynamometer force components. Afterwards, the data is transformed into the frequency domain with a Fast Fourier Transformation and displayed as waterfall plots. Afterwards, several comparisons and plots are processed and visualised, including the calculation of absolute and relative errors between cases A, B and C. An additional case N was introduced during post-processing to evaluate the rotation direction of the flywheel for case A.

3.2.1 Error Case Estimation

The following processing steps provide a meaningful comparison between the different error cases. First, the absolute and relative errors are calculated by subtraction. The error results are displayed in waterfall Plots to analyse the error magnitudes of the

absolute error and the significance of the relative error with regard to the baseline vibration.

Second, the data is transformed using a logarithmic scale in one representation and a square root transformation for a second representation. On one side, the logarithmic scale allows us to focus on the relative changes, especially between values where the difference is large, making small variations more visible. On the other hand, the square root transformation allows for a more intuitive insight, reducing the influence of high values.

As a third step, the transformed data is visualised with heatmaps to present a condensed version of the data, easing the identification of trends while reducing noise and outliers.

Finally, the average magnitude of the noise is estimated for each case. In the first stage, an Interquartile Range (IQR) is selected due to the skewed nature of the data since the nature of the expected data should not be normal-distributed. The first quartile (Q1) and fourth quartile (Q4) are also selected for processing. Afterwards, the mean, median and Root Mean Square (RMS) values are computed for the dataset.

4. Results

The experiment's goal was to evaluate the microvibration profile of the reaction-wheel tested under changing gravity vector conditions. Furthermore, we want to identify the source of the change in the microvibration profile, be it the test-setup behaviour or the device tested, namely the reaction-wheel.

It is to be noted that the facility and the test setup are powered by 230V 50Hz mains electricity. The charge amplifier may record line noise, which is evident in the results, represented by the 50Hz peaks and the resulting harmonics in the FFT.

4.1 Pulse Event Results

This test allows insight into two areas of interest. First, generating the torque pulse may excite different structural elements of the complete setup such that the validation of the measurement can be studied. The effect can be seen in Figure 5, where the harmonics of the systems are made visible. The most relevant harmonics have already been identified in [3], being the elastic rope suspension at 9 Hz and the higher harmonics. The source of a single narrow resonance at 249 Hz could not be identified.

IAC-24-C2.4.2.x88721 Page 5 of 12

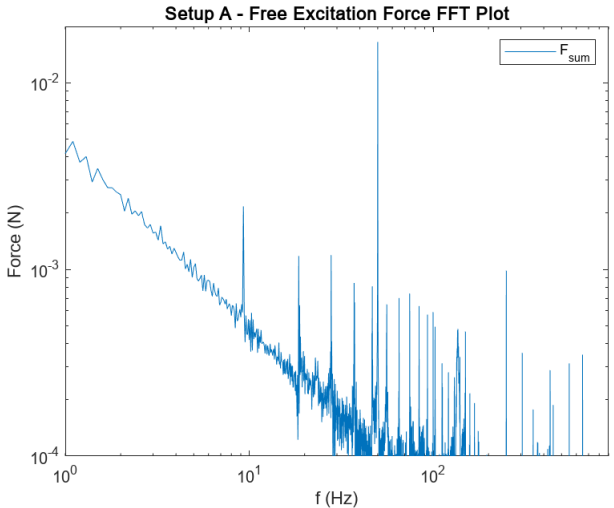


Figure 5: System response of Setup A after a Pulse Event test. The peak at 50Hz is attributed to line noise.

Second, the control system dynamics, such as the system response time and the motor controller control loop frequency, can be evaluated. As shown in Figure 6, the pulse event period achieved last for about 100 milliseconds. After the Motor engages applying a torque, the system oscillates and stabilises around a constant torque in a matter of 60 milliseconds. After the Motor is powered off, the torque drops and the system settles in about 80 milliseconds. Due to proprietary reasons, the exact motor behaviour is not further disclosed.

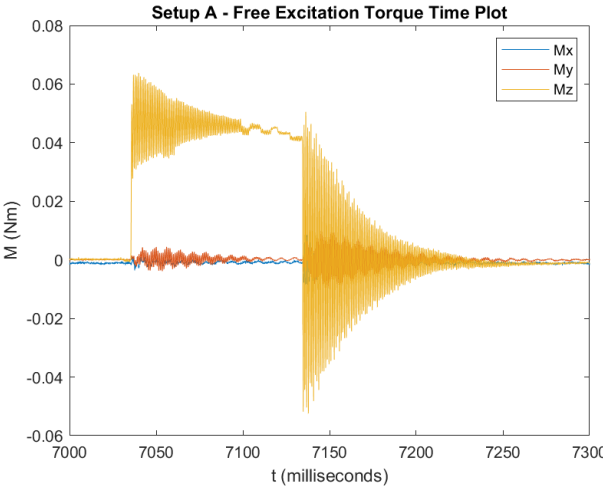
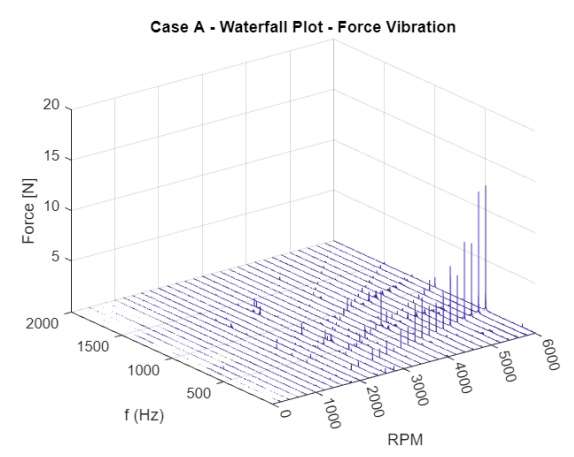


Figure 6: Time-domain plot of the torque at the dynamometer interface during a Pulse Event test

4.2 Continuous Measurements Results

The observation of the different test cases, as seen in the waterfall plots, displayed many expected features like harmonics originating from the structural resonances and imbalance effects emerging from the reaction-wheel, visible both in the force and torque micro-vibration waterfall plots in Figure 7. The microvibration profile is as expected, with an augmentation of the overall magnitude and increasing RPM. A complete set of Data can be found in Appendix A.



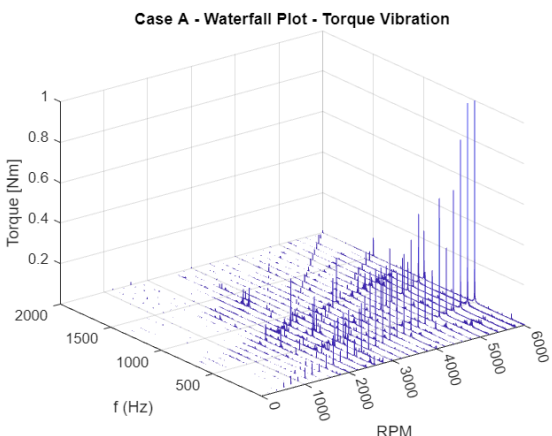


Figure 7: Waterfall Plot representation of the reaction-wheel micro-vibration profile in Case-A

4.2.1 Absolute and Relative Error Comparison

The comparison of the absolute and relative errors between test cases A, B, and C are displayed in waterfall plots and on heat maps, as shown in Figure 8 and Appendix B. The analysis cases are named after the test cases compared, like setup A against setup C in Figure 8.

The interpretation of the unfiltered data is difficult due to the size of the matrices. Furthermore, without proper data filtering, the relative error may be misleading when values are small or near zero. To compensate this both logarithmical and square root filters have been applied to identify points of interest, like in the example in Figure 8, which are later observed in other representations. The causes of these deviations cannot be directly correlated to changes in the system behaviour and may require further study.

IAC-24-C2.4.2.x88721 Page 6 of 12

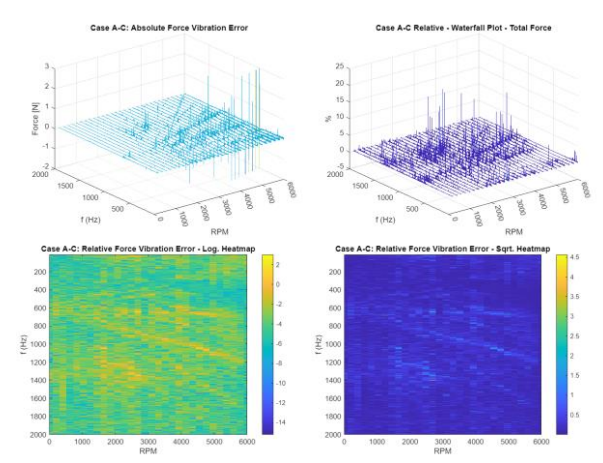


Figure 8: Error estimation A-C between the Setups A and C, with the heatmaps providing guidance to identify areas of interest

4.2.2 Inverted Rotation Direction Comparison

While most of the error cases were analysed using a single rotation speed direction, nominal positive, another case was studied. The first step is to compare the results for the test case Setup A, rotating in the nominal positive direction (from 200 to 6000 RPM), against itself, but using the test data recorded while the reaction-wheel is rotating is operated in the negative direction (from -200 to 6000 RPM), called test Case N, and analyse the relative and absolute error, resulting in the analysis case A-N. The next step would be to compare the error cases A-C, normal and inverted configuration, and N-C.

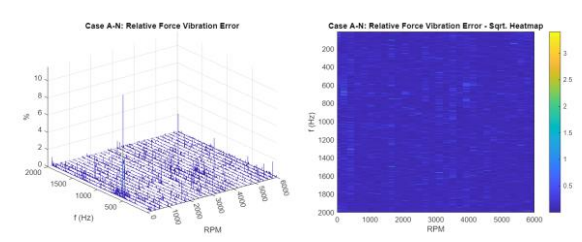


Figure 9: Error case A-N showing no clear patterns on deviations caused by the wheel rotation direction.

The results show that the error case A-N is minimal overall, without showing clear patterns, with the exception of individual outliers, as shown in Figure 9.

On the contrary, if the error case N-C is observed and compared with the case A-C, the data shows an overall higher noise level, as it can be seen in Figure 10. The root cause could not be identified.

4.2.3 Average Magnitude of the Noise

The results of the error computation have been sampled, an extract displayed in Table 2 and provided in Annex C. A trend can be seen where the computed noise levels are lower for test-case N-C opposed to A-C.

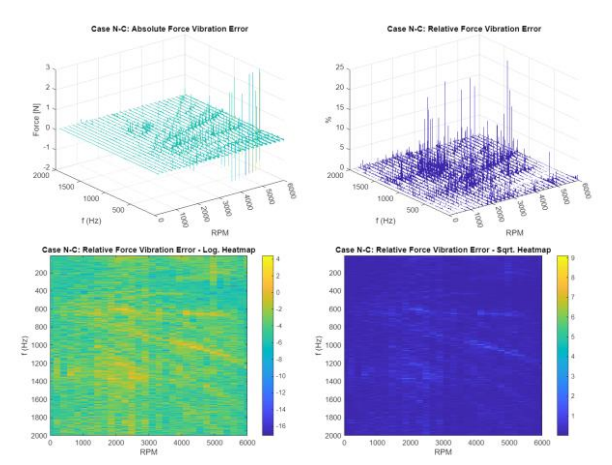


Figure 10: Error case N-C showing similar patterns to the error case A-C but with lower noise on the square-root transformed heatmap (bottom right).

Table 2. Extract of the Analysis Table for Error Comparison, including the error noise magnitudes.

| | 6 | | | |
|--------------------|----------|----------|----------|--|
| Case | Mean | Median | RMS | |
| | Noise | Noise | Noise | |
| A-C Force sqrt. | 0.168900 | 0.141130 | 0.203910 | |
| IQR50 | | | | |
| N-C Force Sqrt. | 0.175830 | 0.147610 | 0.212490 | |
| IQR50. | | | | |
| A-C Force Sqrt.Q1 | 0.053788 | 0.056841 | 0.057056 | |
| N-C Force Sqrt. Q1 | 0.054231 | 0.057404 | 0.057549 | |
| A-C Force Sqrt.Q4 | 0.418440 | 0.356970 | 0.465440 | |
| N-C Force Sqrt. Q4 | 0.438720 | 0.371830 | 0.494200 | |

5. Discussion

B Based on the results, we will first focus on the validity of the overall experimental setup and then discuss the data processing results and analysis.

In general, the experimental setup is centred around the rotation of the gravity vector. While the rotation of the axis is, in fact, a change, it does not fully mimic the micro-gravity state and hence limits the range validity of the results. In contrast, the orientation of the gravity vector may play a role during end-to-end system tests during the micro-vibration test or verification and validation phases of a spacecraft in production, where the integrated reaction-wheels are operated [2].

While the setup is designed to host small—to medium-sized reaction-wheels, structural dynamics may limit its upward scalability. Larger test setups may require new designs to ensure that elements of the setup, like the resonance of the dynamometer's ceramic plate [3], do not limit the measurement range.

As highlighted, the test setup was first validated in [3]. The existence of most harmonics can be backtracked to exist in the general test setup and be, to a large degree, independent from the Device Under Test,

IAC-24-C2.4.2.x88721 Page 7 of 12

in this case, the reaction-wheel operated. This is the case, for example, for the fundamental resonance frequencies emerging from the seismic mass suspended with elastic ropes. A single resonance at 249 Hz was identified, but the source or cause of the resonance could not be found. The impact of this resonance on the overall test is still to be studied.

In the context of the reaction-wheel test itself, the motor controller's system response time may limit the quality of the results achieved during the pulse-event test. Further insight into the reaction-wheel's motor-control dynamics is possible, but the scope of the insight and results cannot be disclosed due to proprietary reasons.

From the continuous measurement results, we can learn that differences and deviations between the test cases, called errors in the realm of this study, may be made visible using different filter and representation methods. Additionally, outliers and noise in the waterfall plots were not further investigated. Due to the experimental nature of this study, further analysis of the root causes of these errors, e.g. through additional simulations and tests, would exceed the scope of work.

6. Conclusions

In summary, this study presented the experimental test case for a reaction-wheel characterization under the change of the gravity vector. It also described the overall feasibility and validity, including the data processing performed and the results on the magnitude of the impact on the testbed and DUT once the gravity vector is rotated.

While individual findings and fault cases, like an unknown, narrow resonance at 249Hz, have to be further investigated, the overall usability of the experimental setup has been validated. Moreover, the further executions of tests and experiments on the testbed may help identify and correct individual fault cases and errors, as well as improve the overall performance of the test setup. A possible identification of the source may be achieved through the use of alternative measurement devices and DUTs to identify potential sources.

Further investigation and development of the command and control signal chain may improve the timing and synchronization issues regarding the reaction-wheel controllability. This may involve implementing a true RTOS Host PC to control the experiment or using a more direct command structure

between the Control Software and the reaction-wheel motor controller.

Additionally, the analysis toolset may be enhanced in the future with methods such as Peak Detection Comparison, Frequency Band Comparison, Cross-Correlation, and Spectral Coherence. It has been found that data processing and analysis generally rely on a script-based toolchain. Further automation and processing pipelines may be implemented to increase the data processing capabilities and, hence, process more experimental and simulated data.

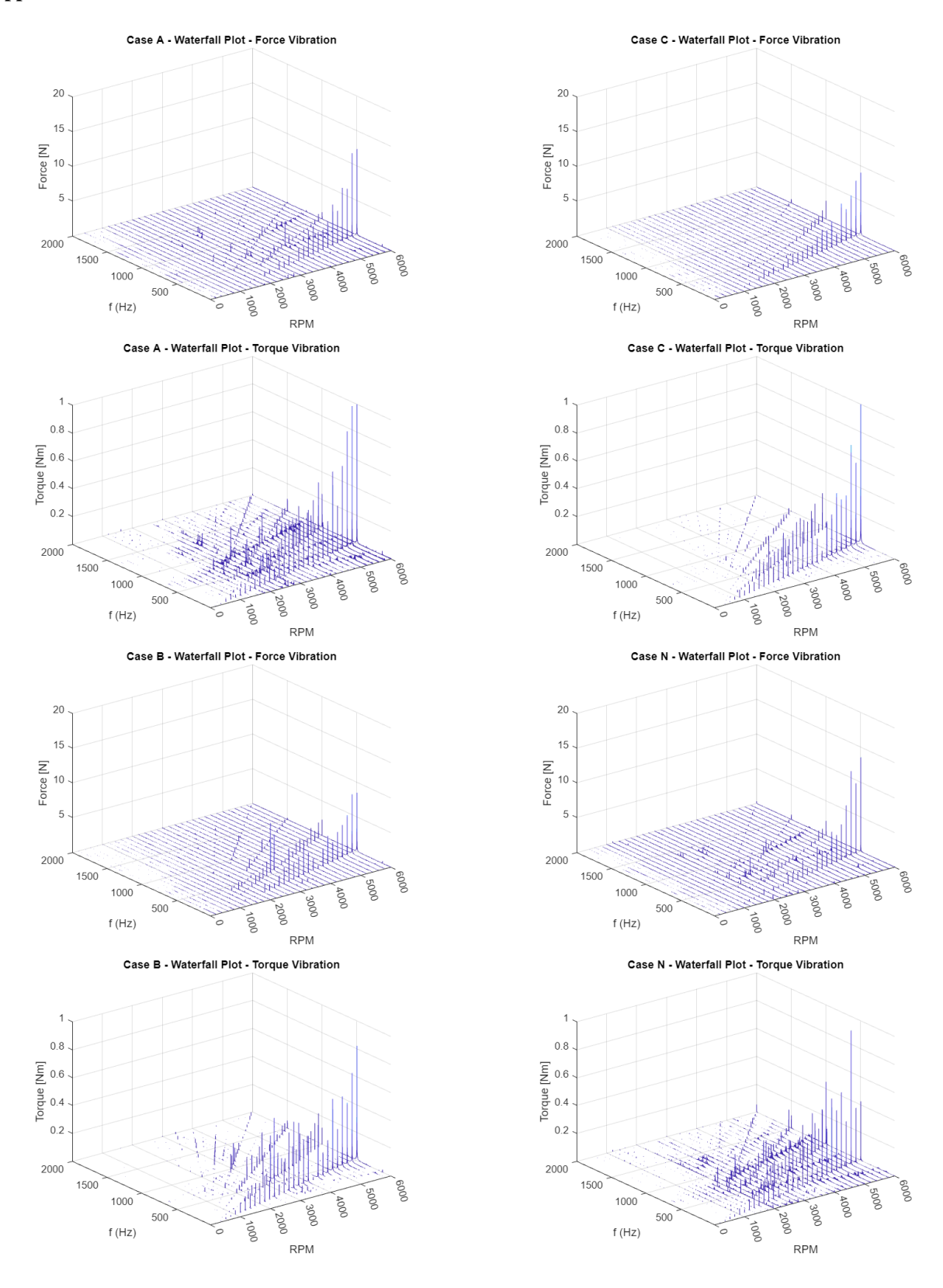
Increasing the quantity of experimental data and overall test-time availability may prove beneficial in studying outliers, noise, and transient events captured during the tests since the repeatability of the tests and long-term measurements could help explain these artefacts.

Conclusively, this study provides new insights into developing tools and methods for micro-vibration characterization, mainly when non-linear effects on harmonics shift, the high-frequency micro-vibration domain, and equipment condition monitoring are investigated. Specifically, micro-vibration management has a significant implication on spacecraft and mission design [1]; hence, the expansion of testing capabilities, as presented here, may open roads to new vibration management techniques. It is to be noted that the gap between the measurement method presented and the validity in contrast to in-orbit or microgravity operations is still a topic to be investigated, especially since the lack of in-flight measurements of microvibrations is still a significant blocking point in microvibration and jitter management, as described in [1].

In the larger context of this study, the behaviour of reaction-wheels and motors is being investigated at the DLR Institute of Space Systems Department for Navigation and Control Systems. Several facilities and resources are available to study and investigate microthe controllability vibrations' impact on management of jitter onboard spacecraft. Furthermore, the goal of developing systems to measure microvibrations is pursued, as in the CubeSat-mission VIBES [5][3] of the City University of Applied Sciences Bremen. Specifically, this includes, among others, support in designing and implementing testbeds for characterizing hardware generating micro-vibrations and preparing end-to-end tests using test actuators and shakers mounted on structures and systems.

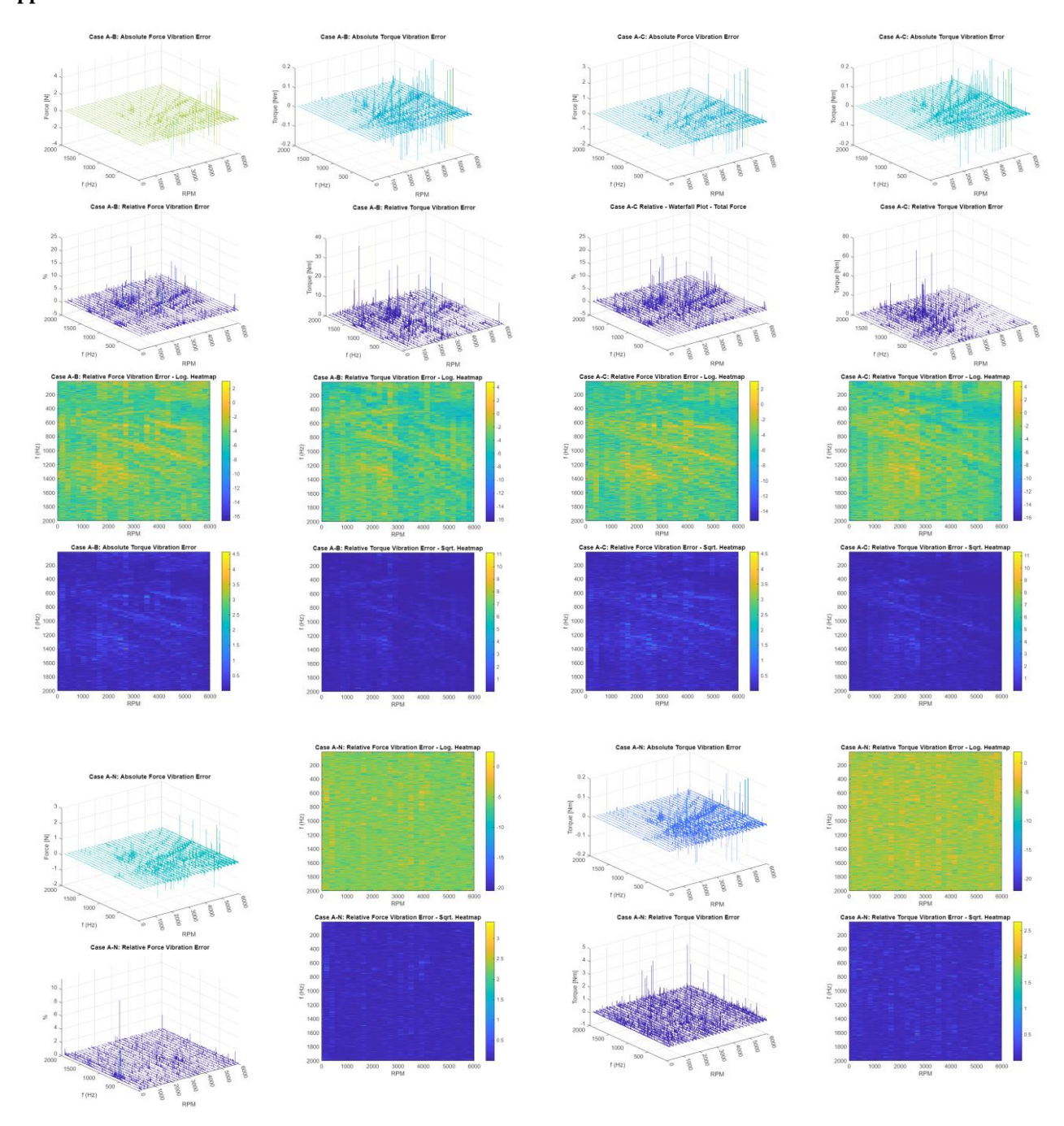
IAC-24-C2.4.2.x88721 Page 8 of 12

Appendix A: Waterfall Plots

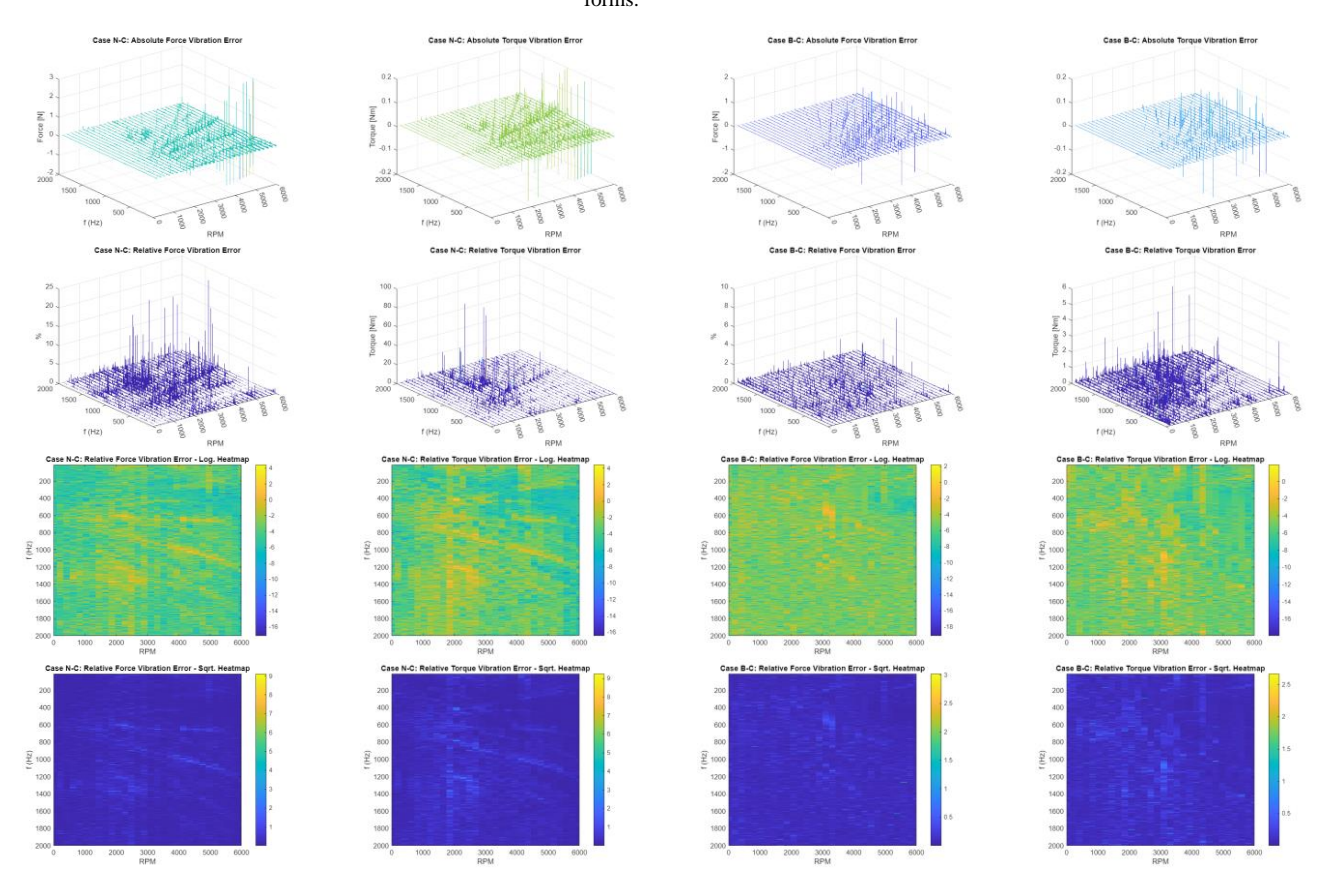


IAC-24-C2.4.2.x88721 Page 9 of 12

Appendix B: Error Case Plots



IAC-24-C2.4.2.x88721 Page 10 of 12



Appendix C: Error Case Analysis Table

Table C1. Noise estimation by case

| Casa | Maan | Madian | RMS | Maan | Madian | RMS | Maan | Median | RMS |
|------------------|----------|----------|----------|----------|----------|----------|---------|---------|---------|
| Case | Mean | Median | | Mean | Median | | Mean | | |
| | (IQR50) | (IQR50) | (IQR50) | (Q1) | (Q1) | (Q1) | (Q4) | (Q4) | (Q4) |
| A-B Force Log. | -3.896 | -3.8017 | 4.2086 | -6.0884 | -5.7897 | 6.1704 | -1.9102 | -2.0768 | 2.0291 |
| A-B Torque Log | -3.2336 | -3.0654 | 3.5848 | -5.5438 | -5.2623 | -5.6416 | -1.7788 | -1.9483 | 1.9321 |
| A-B Force Sqrt. | 0.1689 | 0.14113 | 0.20391 | 0.052402 | 0.055308 | 0.055633 | 0.41253 | 0.35402 | 0.45651 |
| A-B Torque Sqrt. | 0.23108 | 0.2052 | 0.27434 | 0.069471 | 0.071995 | 0.074329 | 0.44699 | 0.37751 | 0.50502 |
| A-C Force Log. | -3.8577 | -3.7584 | 4.168 | -6.034 | -5.735 | 6.116 | -1.8867 | -2.0602 | 2.0105 |
| A-C Torque Log | -2.9582 | -2.795 | 3.3419 | -5.3128 | -5.07 | 5.4209 | -1.6566 | -1.8147 | 1.8408 |
| A-C Force Sqrt. | 0.17097 | 0.144 | 0.20573 | 0.053788 | 0.056841 | 0.057056 | 0.41844 | 0.35697 | 0.46544 |
| A-C Torque Sqrt. | 0.26466 | 0.23478 | 0.3144 | 0.07862 | 0.079263 | 0.08475 | 0.48067 | 0.40359 | 0.5534 |
| A-N Force Log. | -5.1429 | -5.0976 | 5.2217 | -6.7572 | -6.4455 | 6.8309 | -3.6426 | -3.8057 | 3.7272 |
| A-N Torque Log | -5.0823 | -5.0882 | 5.1934 | -6.7988 | -6.4894 | 6.8731 | -3.625 | -3.7817 | 3.7089 |
| A-N Force Sqrt. | 0.073926 | 0.07404 | 0.080214 | 0.037467 | 0.039844 | 0.039721 | 0.17742 | 0.14915 | 0.2051 |
| A-N Torque Sqrt. | 0.078294 | 0.074505 | 0.086929 | 0.036745 | 0.038979 | 0.038992 | 0.17868 | 0.15095 | 0.20308 |
| N-C Force Log. | -3.8115 | -3.7066 | 4.1369 | -6.0192 | -5.7153 | 6.1022 | -1.8018 | -1.9786 | 1.938 |
| N-C Torque Log | -3.11 | -2.9384 | 3.5012 | -5.4822 | -5.2112 | 5.5803 | -1.6317 | -1.7999 | 1.8133 |
| N-C Force Sqrt. | 0.17583 | 0.14761 | 0.21249 | 0.054231 | 0.057404 | 0.057549 | 0.43872 | 0.37183 | 0.4942 |
| N-C Torque Sqrt. | 0.24947 | 0.2185 | 0.29891 | 0.071644 | 0.073859 | 0.076724 | 0.48568 | 0.4066 | 0.55879 |
| B-C Force Log. | -5.1689 | -5.1276 | 5.286 | -6.8435 | -6.5371 | 6.9163 | -3.6217 | -3.7893 | 3.7075 |
| B-C Torque Log | -5.0583 | -5.0873 | 5.1939 | -6.8375 | -6.537 | 6.9097 | -3.5772 | -3.7373 | 3.6688 |
| B-C Force Sqrt. | 0.073482 | 0.072718 | 0.080337 | 0.035914 | 0.038062 | 0.03812 | 0.17938 | 0.15037 | 0.20454 |
| B-C Torque Sqrt. | 0.081491 | 0.074692 | 0.092091 | 0.035966 | 0.038063 | 0.038131 | 0.18396 | 0.15433 | 0.21037 |

IAC-24-C2.4.2.x88721 Page 11 of 12

References

- [1] Dennehy, Wolf, and Swanson. "Spacecraft Line-of-Sight Jitter Management and Mitigation Lessons Learned and Engineering Best Practices," NASA/TM-20210017871, 2021.
- [2] ECSS: Manual (ECSS-E-HB-32-26A) for Space Standardization, E. E. C. ECSS-E-HB-32-26A Space engineering and Spacecraft mechanical loads and analysis handbook 2013.
- [3] Bestard Körner, Identification Method for Gravity Caused Effects During the Characterization of Micro-Vibration Sources, IAC-22-C2.3.5.x72668, IAC. 73rd International Astronautical Congress (IAC), 2022-09-18 - 2022-09-22, Paris, France.
- [4] Garcia, Gust, Basata, Gersting, Deka, Thiele, Salah, Bestard Körner, Runte, and Gonzalez. "VIBES: Visionary Ingenuity Boosting European Spacecraft. Managing Microvibrations for the Future of Spaceflight." Archive of Mechanical Engineering, 2023, 183–97. https://doi.org/10.24425/ame.2023.144819.
- [5] Garcia, Thiele, Gust, Grumme, Bestard Koerner, Runte, and Gonzalez. "VIBES: VISIONARY INGENUITY BOOSTING EUROPEAN SPACECRAFT. DEVELOPMENT OF A LOW-COST MICROVIBRATION MEASUREMENT SYSTEM,", 17th ECSSMET, Toulouse, France, 2023.

IAC-24-C2.4.2.x88721 Page 12 of 12